Author Manuscript

Author Manuscript

Author Manuscript

Author Manuscript

HHS Public Access

Author manuscript

Acta Neuropathol. Author manuscript; available in PMC 2020 February 11.

Published in final edited form as:

Acta Neuropathol. 2020 January ; 139(1): 27–43. doi:10.1007/s00401-019-02075-z.

Evidence of corticofugal tau spreading in patients with frontotemporal dementia

Eun-Joo Kim[1,2], **Ji-Hye L. Hwang**[1], **Stephanie E. Gaus**[1], **Alissa L. Nana**[1], **Jersey Deng**[1], **Jesse A. Brown**[1], **Salvatore Spina**[1], **Myung Jun Lee**[2], **Eliana Marisa Ramos**[4], **Lea T. Grinberg**[1,3], **Joel H. Kramer**[1], **Adam L. Boxer**[1], **Maria Luisa Gorno-Tempini**[1], **Howard J. Rosen**[1], **Bruce L. Miller**[1], **William W. Seeley**[1,3]

[1]Department of Neurology, Memory and Aging Center, University of California, 675 Nelson Rising Lane, San Francisco, CA 94158, USA

[2]Department of Neurology, Pusan National University Hospital, Pusan National University School of Medicine and Medical Research Institute, Busan, Republic of Korea

[3]Department of Pathology, University of California, San Francisco, USA

[4]Department of Psychiatry, David Geffen School of Medicine, University of California Los Angeles, Los Angeles, CA, USA

Abstract

Common neurodegenerative diseases feature progressive accumulation of disease-specific protein aggregates in selectively vulnerable brain regions. Increasing experimental evidence suggests that misfolded disease proteins exhibit prion-like properties, including the ability to seed corruptive templating and self-propagation along axons. Direct evidence for transneuronal spread in patients, however, remains limited. To test predictions made by the transneuronal spread hypothesis in human tissues, we asked whether tau deposition within axons of the corticospinal and corticopontine pathways can be predicted based on clinical syndromes and cortical atrophy patterns seen in frontotemporal lobar degeneration (FTLD). Sixteen patients with Pick's disease, 21 with corticobasal degeneration, and 3 with FTLD-*MAPT* were included, spanning a range of clinical syndromes across the frontotemporal dementia (FTD) spectrum. Cortical involvement was measured using a neurodegeneration score, a tau score, and a composite score based on semiquantitative ratings and complemented by an MRI-based cortical atrophy W-map based on antemortem imaging. Midbrain cerebral peduncle and pontine base descending fibers were divided into three subregions, representing prefrontopontine, corticospinal, and parieto-temporo-occipital fiber pathways. Tau area fraction was calculated in each subregion and related to clinical syndrome and cortical measures. Within each clinical syndrome, there were predicted relationships between cortical atrophy patterns and axonal tau deposition in midbrain cerebral peduncle and pontine base. Between syndromes, contrasting and predictable patterns of brainstem axonal tau deposition emerged, with, for example, greater tau in prefrontopontine fibers in behavioral variant

William W. Seeley, bill.seeley@ucsf.edu.

Electronic supplementary material The online version of this article (https://doi.org/10.1007/s00401-019-02075-z) contains supplementary material, which is available to authorized users.

Publisher's Note Springer Nature remains neutral with regard to jurisdictional claims in published maps and institutional affiliations.

Author Manuscript Author Manuscript Author Manuscript Author Manuscript

FTD and in corticospinal fibers in corticobasal syndrome. Finally, semiquantitative and quantitative cortical degeneration scores predicted brainstem axonal tau deposition based on anatomical principles. Taken together, these findings provide important human evidence in support of axonal tau spreading in patients with specific forms of tau-related neurodegeneration.

Keywords

Tau; Transneuronal; Frontotemporal dementia; Frontotemporal lobar degeneration; Pick's disease; Corticobasal degeneration; MAPT

Introduction

Major neurodegenerative diseases, such as Alzheimer's disease (AD), Parkinson's disease (PD), and frontotemporal dementia (FTD), feature progressive accumulation of disease-specific protein aggregates in selectively vulnerable brain regions. In prion diseases related to PrP protein, the normal cellular protein (PrP^{c}) is converted to a misfolded pathogenic form (PrP^{sc}), which propagates through the recruitment and exponential conversion of PrP^{c} into PrP^{sc} [48]. This prion-based amplification process results in trans-synaptic spreading, and increasing experimental evidence suggests that the misfolded disease proteins in a broader spectrum of neurodegenerative diseases, including β-amyloid (Aβ), tau, α-synuclein, and TAR DNA-binding protein of 43 kDa (TDP-43), exhibit prion-like properties, including the ability to undergo corruptive templating and to propagate along axonal connections [1, 18, 22, 41, 47]. Spreading tau aggregation, for example, can be induced in tau-transgenic mice by the intracerebral injection of brain homogenate from transgenic mice harboring the *MAPT* P301S mutation or human brain tissue from patients with tauopathy [3, 12, 24, 28, 30]. In living patients, evidence for transneuronal spread has come from studies relating patterns of neurodegeneration to functional [21, 63, 72] and structural [50] network connectivity. These studies, while most consistent with a transneuronal spread model, provide only indirect evidence for spread of disease proteins along axonal pathways.

Direct microscopic evidence for transneuronal disease protein spreading remains limited in humans. The hierarchical distribution of protein deposits in AD and PD, as reflected in the staging schemes put forth by Braak et al. [4, 5], suggests the possibility of spreading, but there have been few systematic human studies that relate disease protein aggregation in neurons to the presence of aggregated tau in distal axons known to emanate from those neurons based on clear-cut neuroanatomical principles [49].

To test predictions made by the transneuronal spread hypothesis in human tissues, we evaluated whether tau pathology spreads along the corticospinal and corticopontine pathways in frontotemporal lobar degeneration with tau-immunoreactive inclusions (FTLD-tau). We focused on Pick's disease (PiD), corticobasal degeneration (CBD), and FTLD-tau with *MAPT* pathogenic variants (FTLD-tau/*MAPT*), because these disorders are most likely to arise in the cerebral cortex before spreading to the brainstem in later stages [34, 42, 69]. PiD, CBD, and FTLD-tau/*MAPT* can each present with the behavioral variant of frontotemporal dementia (bvFTD), primary progressive aphasia (PPA), corticobasal syndrome (CBS), or, rarely, progressive supranuclear palsy syndrome (PSP-S, also known as

Author Manuscript Author Manuscript Author Manuscript Author Manuscript

Richardson syndrome, PSP-RS) [23, 35, 37, 46, 52]. We asked whether, across these anatomically distinctive syndromes, cerebral cortical degeneration topography could predict axonal tau deposition topography within the midbrain cerebral peduncle and descending pontine fiber tracts based on the well-known topographical organization of the corticospinal and corticopontine pathways.

Materials and methods

Subject selection

From 437 patients autopsied at the University of California, San Francisco (UCSF) Neurodegenerative Disease Brain Bank (NDBB) between 2004 and 2017, we included those in whom PiD, CBD, or FTLD-tau/*MAPT* was the primary pathological diagnosis. Patients were excluded if they had: (1) no semiquantitative neuropathological assessment, which began in 2008, (2) Braak neurofibrillary tangle stage > 3 [4], (3) Alzheimer's disease neuropathological change (ADNC) > intermediate [27], (4) Lewy body disease (LBD) > brainstem predominant [38], (5) TDP-43 pathology beyond the limbic structures [2], (6) major territorial ischemic infarcts or intracranial hemorrhages in the hemisphere analyzed, or (7) neither midbrain nor pons tissue blocks available for study. Based on these stringent criteria, 16 patients with PiD, 21 with CBD, and 3 with FTLD-tau/*MAPT* (P301L) were included. More specifically, after excluding cases with damaged midbrain and pons materials, 12 PiD, 13 CBD, and 3 FTLD-tau/*MAPT* sections remained for the midbrain analysis and 15 PiD, 21 CBD, and 3 FTLD-tau/MAPT sections remained for the pons analysis (Supplementary Figure, Online resource; Table 1). All patients underwent an extensive dementia-oriented postmortem assessment at UCSF following previous approaches [43, 66].

All patients had undergone neurological evaluation, including extensive neuropsychological assessment and neuroimaging, at least once, at the UCSF Memory and Aging Center. Clinical diagnoses were rendered according to published research criteria for bvFTD [46, 52], PPA [semantic variant PPA (svPPA) and nonfluent/agrammatic variant PPA (nfvPPA)] [23], PSP-RS [35], and probable AD dementia, the latter mentioned here, because one patient with PiD was diagnosed with AD-type dementia (probable AD) during life [39, 40]. Subject demographics, as well as clinical and neuropathological data, are provided in Table 1.

Corticospinal and corticopontine pathway

The corticospinal tract consists of all axonal fibers that arise from neurons in the deeper part of layer 5 in the primary motor area (area 4), the premotor area (area 6), the postcentral gyrus (area 3a, 3b, 1, and 2), and the adjacent parietal cortex (area 5). This tract passes through the medullary pyramid. About 90% of the corticospinal tract crosses at the junction of medullar and spinal cord to form the lateral corticospinal tract. Approximately 8% of the uncrossed fibers form the anterior corticospinal tract and the remaining uncrossed fibers descend into the uncrossed lateral corticospinal tract [9]. The corticopontine fibers arise chiefly from layer 5 pyramidal cells within the frontal, parietal, temporal, and occipital cortices, descend without crossing, and terminate at the pontine nuclei [9]. Although PiD is

Author Manuscript Author Manuscript Author Manuscript Author Manuscript

known to target layers 2 and 6, it also heavily affects layer 5, as does CBD [26, 31]. Tau-positive ballooned neurons in PiD and CBD in fact chiefly occupy layer 5. Corticospinal and corticopontine fibers are topographically organized in the cerebral peduncle and rostral pons. In the cerebral peduncle, the corticospinal fibers occupy approximately the middle third of each crus, the prefrontopontine fibers occupy the medial third, and the parieto-temporooccipital (PTO) fibers occupy the lateral third [53, 65]. In the rostral pons, the corticospinal fibers are found in central parts; the prefrontopontine fibers are found within the medial and ventral parts; and the PTO fibers are found in the lateral and dorsolateral parts of the pons [8, 15, 25, 44, 60] (Fig. 1).

Assessment of cerebral cortical degeneration

Cerebral cortical degeneration was rated using a neurodegeneration score, a tau score, and a composite (neurodegeneration and tau) score, each based on the semiquantitative neuropathological assessment. Eight micron-thick sections from the frontal pole, anterior orbital gyrus, anterior cingulate cortex, middle frontal gyrus, inferior frontal gyrus, subgenual cingulate cortex, inferior temporal gyrus, superior frontal sulcus, entorhinal cortex, superior/middle temporal gyrus, pre/postcentral gyrus, angular gyrus, posterior cingulate cortex, and calcarine cortex were prospectively examined by an experienced investigator (WWS, LTG, or SS). The neurodegeneration, tau, and composite scores were calculated using the following grading system:

1. The Neurodegeneration score (range 0–6) was the mean of the vacuolation and gliosis scores plus the neuronal loss score. Vacuolation, gliosis, and neuronal loss were scored in each section stained with H&E using a three-point grading: none = 0; mild = 1; moderate = 2; severe = 3.

2. For the Tau score (range 0–3), tau-positive inclusions consisted of Pick bodies, astrocytic plaques, thorny astrocytes, tufted astrocytes, neurofibrillary tangles (NFTs), globose tangles (GTs), neuronal cytoplasmic inclusions (NCIs), and other glial cytoplasmic inclusions (GCIs) were counted in the most severely affected 100X microscopic field using the following grading: none = 0; 1–5 inclusions per section = 1; 6–14 inclusions per section = 2; ≥ 15 inclusions per section = 3. The burden of tau gray matter threads (GMTs) or white matter threads (WMTs) was separately graded on an ordinal scale: none = 0; mild = 1; moderate = 2; severe = 3. Each tauopathy has characteristic morphological features. Therefore, the tau score was the mean score among these tau elements (PiD: Pick bodies, NCIs, GCIs, GMTs, WMTs; CBD: astrocytic plaques, thorny astrocytes, tufted astrocytes, NCIs, GCIs, GMTs, WMTs; FTLD-tau/*MAPT* mutation: NFTs, GTs, thorny astrocytes, tufted astrocytes, NCIs, GCIs, GMTs, WMTs). Although the focus of the study is transneuronal spreading of tau, we included both neuronal and glial measures in our regional tau scores, because, in our experience, the combined measures provide the most useful index of overall regional tau burden. Neuron-only composite measures in our database tend to exhibit less dynamic range and may suffer from ceiling and floor effects. Nonetheless, to ensure that the regional tau burden correlations were not overly influenced by non-neuronal measures, we repeated our main analyses based on

Author Manuscript Author Manuscript Author Manuscript Author Manuscript

the neuron-only measures (Pick bodies, NCIs, GMTs, NFTs, and GTs) and noted any discrepancies with the main results.

3. The Composite score was the sum of the neurodegeneration score and the tau score (range 0–9).

The cerebral cortex was partitioned into three broad region groups: frontal, rolandic/perirolandic, and PTO regions, corresponding to the brainstem topography. The regions of interests (ROIs) falling in these broad territories were grouped as follows: Frontal group = frontal pole, anterior orbital gyrus, anterior cingulate cortex, middle frontal gyrus, inferior frontal gyrus, subgenual cingulate cortex, superior frontal sulcus; rolandic/perirolandic group = precentral gyrus, postcentral gyrus; PTO group = inferior temporal gyrus, entorhinal cortex, superior/middle temporal gyrus, angular gyrus, posterior cingulate cortex, and calcarine cortex. The regional group score was calculated as the mean among regions in the group. Therefore, each case had three subregional (frontal, rolandic/perirolandic, and PTO) scores for each measure (neurodegeneration, tau burden, and composite, Table 2).

Assessment of cortical atrophy

Thirty-three out of the forty total patients underwent antemortem structural magnetic resonance imaging (MRI) with a 1.5 or 3 T scanner. If a subject had more than one MRI, then the MRI obtained closest to death was selected. The mean interval from MRI to death was 3.0 ± 2.9 years. Structural T1-weighted images were preprocessed for voxel-based morphometry (VBM) in statistical parametric mapping (SPM) 12 using the segment program with default parameters for bias regularization, tissue-type segmentation, and normalization, aligning to the SPM default healthy adult tissue probability maps. Tissue segmentation maps were then smoothed with an 8 mm Gaussian kernel. Next, focusing on brain regions sampled in the UCSF NDBB, we generated a W score map for each patient compared to 288 clinically normal controls. Specifically, to assess imaging-pathology correlations at the single subject level in each of the 27 histological ROIs (Supplementary Table, Online resource), we used a standardized algorithm for identifying the imaging ROI that best matched our standard neuropathological dissections, similar to previous approaches [51]. To create a standard set of ROIs for this and future studies, we elected to use the Human Brainnetome Atlas, a validated connectivity-based parcellation atlas composed of 210 cortical and 36 subcortical brain regions, classified by means of noninvasive multimodal structural, task-free functional, and diffusion MRI methods [20]. This atlas does not contain parcels for the cerebellum and the brainstem; therefore, dentate nucleus, substantia nigra, and tectum ROIs were manually drawn on the MNI T1 template using MRIcron mirroring our standard blocking protocol [54]. To select Brainnetome parcels that best matched our remaining standard histological dissections, we first used MRIcron to manually draw MNI T1 template ROIs mirroring our standard dissections. We then assigned each drawn ROI to the Brainnetome parcel with the highest voxel overlap in MNI space. Fifteen drawn ROIs were uniquely assigned to a single Brainnetome parcel. Drawn ROIs covering amygdala, superior/middle temporal gyrus, thalamus, calcarine cortex, and entorhinal cortex were better represented by combining 2–3 Brainnetome parcels each to cover the entire volume of the region assessed neuropathologically (Supplementary Table, Online resource). Suitable Brainnetome parcels matching the standard dissections of the frontal pole, globus pallidus,

Author Manuscript Author Manuscript Author Manuscript Author Manuscript

and subthalamic nucleus were not available; therefore, for these regions, we used the drawn ROI parcels. Drawn ROI parcels were also used for the dentate nucleus, substantia nigra, tectum, and periaqueductal gray, which are not represented in the Brainnetome atlas. The substantia nigra ROI included the entire extent of the nuclei bilaterally. The final list of Brainnetome parcels corresponding to brain ROIs is provided in the Supplementary Table, Online resource. Once all ROIs were chosen, we extracted the meanW score for each region-of-interest (i.e., parcel) from the left and right hemisphere for every subject, using methods previously described [32]. The *W* score map of each subject was first downsampled to a 2-mm voxel resolution to match the resolution of the parcels. The program fslstats from FSL 5.0.9 was then used to calculate the mean W score for each parcel by taking the sum of the values of all non-zero voxels within the parcel and dividing it by the number of non-zero voxels within the parcel. To calculate the regional (frontal, rolandic/perirolandic, and PTO) atrophy scores, we averaged the mean *W* scores for each parcel within a group, with parcels grouped in the same manner used to assess cerebral cortical degeneration.

Assessment of brainstem corticospinal and corticopontine tract tau pathological burden

First, 10-μm-thick midbrain and pons sections were stained for hyperphosphorylated tau (CP-13 antibody, courtesy of Peter Davies) without counterstaining. A total of 67 sections were assigned to one of three consecutive tau immunostaining runs, with a 1-month interval between runs (first run, 26 sections; second run, 37 sections; third run, 4 sections). We originally designed the study with only FTLD-tau pathology presenting as bvFTD and CBS (first run). Then, we expanded the initial subject population to FTLD-tau presenting with any clinical syndrome and included newly autopsied bvFTD and CBS subjects (second run). Finally, we added a few more patients newly autopsied within the period of study (third run). Five randomly selected cases from the first run had adjacent (serial) midbrain sections stained in the second run. The intraclass correlation coefficient (absolute agreement model) was 0.979 (95% CI 0.822–0.998, $p = 0.002$) between tau area fractions (%) from batch 1 and batch 2 sections. We did not examine batch effects between runs 2 and 3, because we were not expecting to include a third run, which was small (4 sections) and added to allow us to incorporate a few additional subjects who became eligible after study launch. Next, all stained sections were scanned using a 10 × objective on a Zeiss Axioscan slide scanner. Color CZI images were converted to 8-bit greyscale TIF images for analysis in Image J. ROIs were drawn, using Image J, around the cerebral peduncle or pontine fibers ipsilateral to the side assessed for neuropathological diagnosis, typically the more affected hemisphere. In eight cases, the ipsilateral cerebral peduncle was not usable, and in two cases, the ipsilateral pons was not usable due to tissue damage, so the contralateral side was used. The midbrain cerebral peduncle was divided into three portions (prefrontopontine fibers, M1; corticospinal fibers, M2; PTO fibers, M3) of equal horizontal dimensions based on a line connecting the most medial and lateral points of the peduncle (Fig. 2a), following previous approaches used to subdivide the corpus callosum [70]. The drawing of ROIs for the pontine fibers was based on several atlases or studies regarding the organization of the corticopontine fibers, showing the position, in the axial plane, of the prefrontopontine fibers (P1), the corticospinal fibers (P2), and the PTO-pontine fibers (P3), which follow a medial-to-lateral topography [15, 25, 44, 67]. In contrast to the cerebral peduncle ROIs, pontine fiber ROIs were drawn based on darkfield images, which allowed for enhanced visualization of the fiber pathways (Fig. 2b).

Author Manuscript Author Manuscript Author Manuscript Author Manuscript

The tau area fraction (%) for each ROI was derived after thresholding tuned to our staining characteristics in traced regions using the Yen algorithm. Unlike the singular M1, M2, and M3 ROIs, each P1, P2, or P3 ROI was composed of multiple ROIs (Fig. 2b). Thus, the tau area fraction (%) for P1, P2, and P3 was calculated by dividing the summed total tau-positive pixels across all P1, P2, or P3 ROIs by the summed total areas within P1, P2, or P3. All of these procedures were carried out by a single examiner, who was blind to clinical and pathological diagnoses.

Statistical analysis

Friedman's ANOVA test and the Wilcoxon test were used to compare the tau area fractions within each ROI according to the clinical syndromes, bvFTD and CBS. The Mann–Whiney U test and Fisher's exact test were used to compare the rank order of three of the cerebral peduncle or pontine fiber ROIs between bvFTD and CBS. Because cortical tau, neurodegeneration, and composite scores were originally obtained using an ordinal scale, and were highly variable between subjects, the raw or rank values between subjects did not show a linear correlation. Therefore, correlations between the rank orders among the indices of cortical degeneration in each anatomical region (frontal, rolandic/perirolandic, or PTO region) and tau pathology in the three subregions of midbrain cerebral peduncle and basal pontine descending fibers were assessed with Spearman's rank-order correlation statistic. Statistical analysis was performed using SPSS 23. A value of $p < 0.05$, two-tailed, was considered significant.

Results

Clinical syndrome predicts brainstem axonal tau deposition topography

Figure 1 illustrates the association between cortical atrophy patterns and tau deposition in the midbrain cerebral peduncle and pontine descending fibers in each clinical syndrome. For bvFTD, given its known pattern of frontal-predominant degeneration, the transneuronal framework predicts that pathological tau originating within frontal subcerebral projection neurons will propagate along prefrontopontine axonal fibers, which are localized in the medial portions of the cerebral peduncle and pons. Indeed, in bvFTD, the most prominent axonal phospho-tau deposition was identified in these regions. Likewise, in CBS, a perirolandic syndrome targeting the primary motor and somatosensory cortices, we observed tau deposition in axons comprising the middle portions of the cerebral peduncle and pons. In bvFTD due to FTLD-tau/*MAPT*, which features severe frontal and temporal atrophy, profound tau deposition was observed in both posterolateral and medial portions of the cerebral peduncle and pontine descending fibers (Fig. 1).

To quantify these observations and formally test the predictions made by the transneuronal spreading model, we first investigated whether tau area fraction differed in the M1, M2, and M3 areas within clinical syndromes, focusing on bvFTD and CBS in light of their suitable sample sizes and clear-cut anatomical predictions.

Consistent with our predictions, in bvFTD, axonal tau fraction significantly differed among the M1, M2, and M3 areas (Friedman test, $\chi^2 = 18.14$, $df = 2$, $p < 0.001$). Post hoc analysis

Author Manuscript Author Manuscript Author Manuscript Author Manuscript

confirmed that tau area fraction was significantly greater in M1 than in the M2 or M3 areas, whereas M2 and M3 did not differ (M1 vs. M2, $p = 0.001$; M1 vs. M3, $p = 0.001$; M2 vs. M3, $p = 0.594$). In CBS, there was a trend towards an overall difference in tau area fraction between the M1, M2, and M3 areas (Friedman test, $\chi^2 = 5.2$, $df = 2$, $p = 0.074$). Post hoc pairwise comparisons revealed a significant difference in tau area fraction between the M2 and M3 ROIs (M1 vs M2, $p = 0.225$; M1 vs M3, $p = 0.893$; M2 vs M3, $p = 0.043$). Results for the descending pontine fibers were similar. In bvFTD, there was significant difference among tau area fractions in the P1, P2, and P3 areas (Friedman test, $\chi^2 = 13$, $df = 2$, $p = 0.002$). Post hoc analysis demonstrated greater tau area fraction in P1 than in P2 and P3 ROIs, with a trend towards a greater tau burden in P3 than P2 ROIs (P1 vs P2, $p = 0.001$; P1 vs P3, $p = 0.030$; P2 vs P3, $p = 0.064$). In CBS, however, there were no significant differences in the tau area fraction among P1, P2, and P3 ROIs (Friedman test, $\chi^2 = 0.182$, $df = 2$, $p = 0.913$), perhaps because the pons was largely spared of axonal tau deposition (Fig. 3a, b).

Next, we asked whether the axonal phospho-tau deposition within each midbrain and pons subregion differed between clinical syndromes. Due to the significant between-subject variability in overall tau burden, and because our hypotheses pertained to the relative but not absolute involvement of the different midbrain and pons subregions, for these analyses, we ranked subregions within subjects and compared ranks for each subregion between clinical syndromes. Consistent with our hypotheses, ranks of tau area fraction in M1 and M2 differed between bvFTD and CBS, whereas the M3 ROI did not (M1, $U = 8.5$, $p = 0.001$; M2, $U = 5.5$, $p = 0.004$; M3, $U = 29.0$, $p = 0.521$). Tau area fraction in M1 ranked highest in bvFTD, but in CBS, M2 tau fraction ranked highest. In other words, although tau area fraction in M1, M2, and M3 did not differ statistically in CBS (Fig. 3b), the rank of the M2 tau in CBS was higher than in bvFTD, consistent with our hypotheses (Fig. 3c). In the descending pontine fibers, tau area fraction in P2 was higher than in the other ROIs in CBS and in bvFTD (P1, $U = 47.0$, $p = 0.053$; P2, $U = 34.0$, $p = 0.010$; P3, $U = 75.5$, $p = 0.930$) (Fig. 3d).

Although the PPA, PSP-RS, and AD-type dementia syndromic groups were too small to afford statistical comparisons, each was associated with a predictable pattern of axonal tau deposition in the brainstem (Fig. 4). The nfvPPA (2 PiD, 2 CBD) and the PSP-RS groups (3 CBD), each had the most tau in M1, reflecting their frontal-predominant topography [10, 33, 56], whereas in svPPA (1 PiD, 1CBD), tau was concentrated in M3, reflecting its temporal-predominant pattern. Likewise, nfvPPA (4 PiD, 3 CBD) and PSP-RS (3 CBD) had the greatest amount of tau in the P1 area, whereas in the one patient with an AD-type (temporal/parietal-predominant) dementia due to underlying PiD, the greatest tau burden was observed in the P3 area, through which the PTO-pontine fiber course.

Midbrain and pontine tract axonal tau deposition correlates with ante-mortem MR atrophy and post-mortem cortical degeneration and tau inclusion burden

Table 2 indicates cortical degeneration and tau inclusion burden according to clinical syndrome (bvFTD vs. CBS) and FTLD-tau subtype. Regardless of the FTLD-tau subtype, in general, bvFTD had higher frontal tau burden and degeneration scores, whereas CBS

Author Manuscript Author Manuscript Author Manuscript Author Manuscript

showed higher rolandic/perirolandic tau burden and degeneration scores. Next, we sought to relate regional cortical degeneration and tau burden to brainstem axonal tau deposition. We assessed cortical degeneration with quantitative antemortem MRI and with semi-quantitative ratings of post-mortem histology. Cortical tau burden was also semi-quantitatively rated based on tau immunohistochemistry. When collapsed across relevant regions, antemortem and postmortem measures were strongly correlated, as expected (Table 3). Next, we examined the relationship between these cortical measures and the severity of axonal tauopathy within each brainstem subregion. Across all subjects ($n = 28$), M1 tau area fraction correlated with the frontal tau score ($\rho = 0.435$, $p = 0.021$) and the frontal neurodegeneration score ($\rho = 0.556$, $p = 0.002$), but showed only a trend toward a correlation with the frontal composite score ($\rho = 0.339$, $p = 0.078$) and MR atrophy ($\rho = 0.354$, $p = 0.090$) scores. Tau area fraction in M2 correlated with all perirolandic/rolandic neurodegeneration indices (tau score: $\rho = 0.397$, $p = 0.037$; neurodegeneration score: $\rho = 0.493$, $p = 0.008$; composite score: $\rho = 0.529$, $p = 0.004$) except the MR atrophy score, which showed a similar trend (MR atrophy score: $\rho = 0.352$, $p = 0.092$). Tau area fraction in M3 did not correlate with cortical neurodegeneration indices of the PTO areas, perhaps because limited M3 tauopathy was observed overall and only in some syndromes (tau score: $\rho = -0.198$, $p = 0.313$; neurodegeneration score: $\rho = 0.184$, $p = 0.348$; composite score: $\rho = 0.135$, $p = 0.495$, MR atrophy score: $\rho = 0.098$, $p = 0.650$). In the pons ($n = 39$), findings followed a similar pattern, with tau in the P1 subregion correlating with the frontal tau score ($\rho = 0.558$, $p < 0.001$), the frontal neurodegeneration score ($\rho = 0.507$, $p = 0.001$), and atrophy score ($\rho = 0.506$, $p = 0.003$) and showing a trend toward correlation with the composite score ($\rho = 0.313$, $p = 0.052$). Tau area fraction in P2 correlated with composite scores ($\rho = 0.340$, $p = 0.034$). There were trends toward a correlation between tau in P2 and tau score ($\rho = 0.297$, $p = 0.070$) and neurodegeneration score ($\rho = 0.284$, $p = 0.080$) in perirolandic/rolandic regions. Again, tau area fraction in P3 did not correlate with cortical neurodegeneration indices in the PTO areas (tau score: $\rho = -0.053$, $p = 0.748$; neurodegeneration score: $\rho = 0.197$, $p = 0.230$; composite score: $\rho = 0.203$, $p = 0.216$, atrophic score: $\rho = 0.165$, $p = 0.368$) (Table 4).

Relationship between axonal tau deposition in midbrain cerebral peduncle and caudal descending pontine fibers and pontine nuclei

Finally, we explored associations between tau deposition in midbrain cerebral peduncle and pontine fibers in 18 subjects for whom both midbrain and pons sections were available from the same hemisphere (Table 1). There were no significant differences between the tau ranks in the M1 and the P1 areas ($Z = -0.414$; $p = 0.679$), or between the M2 and P2 areas ($Z = -1.111$; $p = 0.267$), or between the M3 and P3 areas ($Z = -0.370$; $p = 0.711$). Figure 5 shows the correlations between the six ROIs and suggests, as predicted by our model, that correlations are strongest within fiber groups known to receive efferent axons from the same cortical sources. Even the lowest correlations are nonetheless high, as might be expected, since regions in all three sectors are typically affected to some degree in each patient.

The analyses presented above focused on axons descending from predictable cortical efferent sources. The findings suggest that tau spreads from proximal cortical neurons into distal portions of axons emanating from those neurons. These data do not, however,

Author Manuscript Author Manuscript Author Manuscript Author Manuscript

determine whether tau moves trans-synaptically from corticofugal neurons to the next neuron in the network. As a final step, we evaluated whether our human materials were consistent with this possibility. We found, in all forms of FTLD-tau we studied, that tau NCIs were frequent within neurons of the pontine nuclei and that, qualitatively, the proportion of NCIs was closely linked to the abundance of tau-positive axonal fibers quantified in the main analyses (Fig. 6).

Discussion

Transneuronal spreading has emerged as prominent framework for understanding tauopathy progression, but to date, little direct human evidence has addressed this concept. Here, we tested predictions made by the transneuronal spread hypothesis using post-mortem materials that allowed us to quantify pathological axonal tau within specific, topographically organized projection pathways. Consistent with a transneuronal framework, we found that syndrome-specific patterns of cortical tau deposition and neurodegeneration strongly predicted tau deposition in brainstem white matter pathways. These data provide novel and compelling human neuropathological evidence for axonal tau spreading, arguably the most direct evidence for this framework in humans to date.

Each histopathological subtype of FTLD-tau can manifest in anatomically diverse clinical syndromes. For example, the two sporadic primary tauopathies studied here, PiD and CBD, can each manifest as bvFTD or CBS but also nfvPPA, svPPA, and other FTD syndromes. According to the network degeneration principles put forth by our group [64], the clinical syndrome reflects the anatomical locus or “epicenter” where tau aggregation begins. The connections of each patient’s epicenter, in turn, influence where the tau will spread via the axonal pathways emanating from the epicenter. Evidence for this framework has come primarily from (1) network-based neuroimaging studies [21, 63, 72], which have used the brain’s healthy connectional architecture to predict spatial neurodegeneration patterns and (2) neuropathological staging efforts, which have been used in an attempt to infer a spatiotemporal progression by studying how regional tauopathy patterns differ across large groups of individuals, many with preclinical neuropathological lesions [4–7].

The transneuronal spread hypothesis has been tested in vivo using transgenic mouse models [45]. Direct injections of synthetic preformed tau fibrils, extracts from transgenic mouse brains, or human brain extracts from patients with tauopathy all induce tau aggregation and propagation from the injection site to even distant, neuroanatomically connected brain regions, most prominently in mice expressing mutant forms of tau [3, 12, 13, 28–30]. Likewise, focal expression of human P301L tau in mouse entorhinal cortex drives tau aggregate formation that spreads over time to the anatomically connected subiculum, dentate gyrus, and hippocampal CA1 and CA3 despite the absence of transgene expression within those regions, consistent with trans-synaptic spread [14, 36]. Despite these pioneering advances, the transgenic mouse models using heterologous promoters result in tau overexpression, creating some uncertainty regarding whether the mouse model findings can be confidently transferred back to patients with tauopathy [45]. Other models based in simpler organisms or cell-based assays likewise require human validation [11, 71]. The present study helps to address this critical issue in the field.

Author Manuscript Author Manuscript Author Manuscript Author Manuscript

A recent report based on a similar framework to ours examined tau deposition in the optic pathway, including the optic nerve, lateral geniculate nucleus (LGN), and occipital cortex [49]. The study included 47 patients with diverse tauopathies (AD, argyrophilic grain disease or “PSP-like” pathology with or without AD-related changes) and found that tau aggregation in the LGN correlated with tau in the occipital cortex and significantly correlated with Braak stage in patients with AD only. Because the majority of the patients in the study had AD, it is not surprising that tau pathological burden in any region would correlate with Braak stage or tau in occipital cortex, which is an area affected in Braak stage VI, and no regions outside the visual pathway were included for comparison. Optic nerve samples were examined only in eight subjects and tau immunoreactivity could not be rated or quantified, because it was so sparse in optic nerve and LGN. The present study, in contrast, used semiquantitative and quantitative methods and related axonal tau deposition to distinct cortical patterns using both between-group and within-subject analyses.

Corticospinal and corticopontine fibers make ideal anatomical pathways in which to test the tau-transneuronal spreading hypothesis, because their anatomical organization is relatively straightforward, even in humans. Previous studies of CBD presenting as CBS demonstrate selective degeneration of the corticospinal pathway (M2) in the cerebral peduncle [53], but this study was performed long before tau was even identified as a major disease protein. We focused the present study on PiD, CBD, and FTLD-tau/MAPT, because they each show profound cortical and brainstem tauopathy and are widely hypothesized to begin in the cortex. We omitted patients with a pathological diagnosis of PSP, because cortical tau and atrophy can be sparse, even in patients with non-Richardson syndromes. Although patients with PSP presenting with non-Richardson syndromes show more cortical tauopathy than do patients with PSP-RS [16, 68], these syndromes could still arise within the topographically organized subfields of the pallidum or subthalamic nucleus. At a minimum, the anatomical literature on these non-Richardson syndromes is still evolving, and we opted to focus on the tauopathies we deemed most straightforward to interpret. Formally studying subcortical-to-cortical spread in PSP represents an interesting potential topic for future research.

In the present study, we first investigated whether bvFTD and CBS would be associated with contrasting and predictable brainstem axonal tau deposition based on the primary locus of cortical neurodegeneration in frontal (bvFTD) vs. rolandic/perirolandic (CBS) cortices. These predictions were strongly supported by visual examination of the tissues (Fig. 1) and by our quantitative data from the midbrain cerebral peduncle. In the descending pontine fibers, patients with bvFTD showed conspicuous tau deposition in the P1 portion, as predicted, but, contrary to our expectations, in CBS, a P2-predominant tau pattern was not demonstrated quantitatively. There are several possible explanations for why pontine axonal tauopathy did not reflect our predictions in CBS. In the monkey, the basis pontis receives topographically organized projections with: (1) the prefrontopontine terminations located in the paramedian nucleus and medial parts of the peripeduncular nucleus in the rostral pons; (2) the motor and sensory corticopontine projections located in a central ‘core’, preferentially in the caudal half of the pons; and (3) the posterior parietal, superior temporal, parahippocampal, and parastriate projections placed more laterally [8, 58, 59, 61, 62]. Although topographical organization of the corticopontine pathways cannot be studied using axonal tracers in humans, lesion studies and neuroimaging research using diffusion tensor

Author Manuscript Author Manuscript Author Manuscript Author Manuscript

resonance magnetic imaging (DTI) have indicated that the human corticopontine projections are organized in a manner similar to that observed in the monkey [15, 25, 44, 57]. For example, one probabilistic DTI-based fiber tracking study found that prefrontopontine fibers preferentially terminate within the medial part of the pons, whereas temporooccipital fibers end in lateral and dorsolateral parts of the pons, and corticospinal and corticobulbar fibers were traced in the middle portion of the ventral pons [25]. Our selection of pontine fiber ROIs relied on data obtained in these studies and, additionally, was designed to reduce bias and promote reproducibility by evenly dividing the pontine base into three segments from medial to lateral. This approach was no doubt subject to potential misclassification of the pontine fibers, which could have contributed to our inability to detect a P2 tau-predominant pattern in CBS; on the other hand, pontine axonal tau deposition was mild across segments, potentially contributing to the lack of a clear signal at this level, which may have been somewhat rostral to where most motor and sensory corticopontine fibers terminate [62]. This study also failed to detect a correlation between the neurodegenerative indices in the PTO area and tau deposition in the midbrain M3 and pons P3 areas. The occipital cortex is typically spared from most neurodegenerative diseases, including PiD and CBD. Therefore, neurodegenerative indices of the PTO regions, because they evenly weighed parietal, temporal, or occipital regions, may not have accurately reflected the severity of neurodegeneration.

Several methodological limitations should be noted. First, the small number of subjects of the same clinical syndrome within each pathological group prevented us from investigating the interactions between clinical syndromes and underlying tauopathy. Distinct FTLD tauopathies may represent distinct strains [19, 55], which could influence transneuronal spreading behavior. The overall hypothesis we sought to test, however, was that tau, regardless strain or species, would show similar, anatomically guided corticofugal spreading behavior, and our results support that hypothesis across three major primary tauopathies, increasing the generalizability of the findings. Second, we concede that although the ROI drawing was done by a single rater, the intra-rater reliability of the drawing procedure remains unquantified. The approach involved relatively few subjective decisions, however, because unbiased quantitative methods were used to divide the cerebral peduncle and pontine fibers into the three sectors used for hypothesis testing. Examiners prospectively rated neuropathological features blinded to study hypotheses, but the use of three examiners over an extended period raises the possibility of inter-rater inconsistency. Monthly consensus meetings are used to enhance cohesion in approach, as are periodic inter-rater reliability exercises, but we acknowledge the possibility of unmeasured inter-rater variation. Third, we acknowledge that there may be a minor contribution from non-axonal elements, such as astroglial and oligodendroglial processes [17], to the white matter tau area fraction data quantified within the midbrain and pons. Inclusion of these elements, however, likely contributed no more than minor noise to the data set given the predominance of axonal tau within our ROIs (Fig. 2). Finally, although the microscopy methods used here were sufficient to address the research questions, future studies could use more quantitative methods (for measuring cortical tau burden) or higher resolution microscopy (for assessing brainstem axonal tauopathy).

Author Manuscript Author Manuscript Author Manuscript Author Manuscript

Summary

With the few exceptions noted, our overall findings fit together into a pattern that strongly supports the tau-transneuronal spreading hypothesis in humans. This work has important implications for modeling disease progression in FTLD-tau and other forms of tauopathy, and we hope that the present framework can inform studies of other major molecular classes of neurodegenerative disease.

Supplementary Material

Refer to Web version on PubMed Central for supplementary material.

Acknowledgements

We thank our patients and their families for participating in neurodegeneration research. We thank Norbert Lee and Anna Karydas for technical assistance.

Funding

Funding was provided by Financial Supporting Project of Long-term Overseas Dispatch of PNU's Tenure-track Faculty (2015) to Eun-Joo Kim, National Institute on Aging (AG023501, AG019724), Tau Consortium, and Bluefield Project to Cure FTD to William W. Seeley and Bruce L. Miller.

References

1. Aguzzi A (2009) Cell biology: beyond the prion principle. Nature 459:924–925 [PubMed: 19536253]
2. Amador-Ortiz C, Lin WL, Ahmed Z, Personett D, Davies P, Duara R et al. (2007) TDP-43 immunoreactivity in hippocampal sclerosis and Alzheimer's disease. Ann Neurol 61:435–445 [PubMed: 17469117]
3. Boluda S, Iba M, Zhang B, Raible KM, Lee VM, Trojanowski JQ (2015) Differential induction and spread of tau pathology in young PS19 tau transgenic mice following intracerebral injections of pathological tau from Alzheimer's disease or corticobasal degeneration brains. Acta Neuropathol 129:221–237 [PubMed: 25534024]
4. Braak H, Braak E (1991) Neuropathological stageing of Alzheimer-related changes. Acta Neuropathol 82:239–259 [PubMed: 1759558]
5. Braak H, Del Tredici K, Rüb U, de Vos R, Jansen Steur E, Braak E (2003) Staging of brain pathology related to sporadic Parkinson's disease. Neurobiol Aging 24:197–211 [PubMed: 12498954]
6. Braak H, Thal DR, Ghebremedhin E, Del Tredici K (2011) Stages of the pathologic process in Alzheimer disease: age categories from 1 to 100 years. J Neuropathol Exp Neurol 70:960–969 [PubMed: 22002422]
7. Brettschneider J, Del Tredici K, Lee VM, Trojanowski JQ (2015) Spreading of pathology in neurodegenerative diseases: a focus on human studies. Nat Rev Neurosci 16:109–120 [PubMed: 25588378]
8. Brodal P (1978) The corticopontine projection in the rhesus monkey. Origin and principles of organization Brain 101:251–283 [PubMed: 96910]
9. Carpenter MB (1991) Core text of neuroanatomy. Williams & Wilkins, Baltimore
10. Caso F, Gesierich B, Henry M, Sidhu M, LaMarre A, Babiak M et al. (2013) Nonfluent/agrammatic PPA with in-vivo cortical amyloidosis and Pick's disease pathology. Behav Neurol 26:95–106 [PubMed: 22713404]
11. Cearley CN, Wolfe JH (2007) A single injection of an adeno-associated virus vector into nuclei with divergent connections results in widespread vector distribution in the brain and global correction of a neurogenetic disease. J Neurosci 27:9928–9940 [PubMed: 17855607]

Author Manuscript Author Manuscript Author Manuscript Author Manuscript

12. Clavaguera F, Akatsu H, Fraser G, Crowther RA, Frank S, Hench J et al. (2013) Brain homogenates from human tauopathies induce tau inclusions in mouse brain. Proc Natl Acad Sci USA 110:9535–9540 [PubMed: 23690619]
13. Clavaguera F, Bolmont T, Crowther RA, Abramowski D, Frank S, Probst A et al. (2009) Transmission and spreading of tauopathy in transgenic mouse brain. Nat Cell Biol 11:909–913 [PubMed: 19503072]
14. de Calignon A, Polydoro M, Suarez-Calvet M, William C, Adamowicz DH, Kopeikina KJ et al. (2012) Propagation of tau pathology in a model of early Alzheimer's disease. Neuron 73:685–697 [PubMed: 22365544]
15. DeArmond SJ, Fusco MM, Dewey MM (1989) Structure of the human brain, a photographic atlas. Oxford University Press, Oxford
16. Dickson DW, Ahmed Z, Algom AA, Tsuboi Y, Josephs KA (2010) Neuropathology of variants of progressive supranuclear palsy. Curr Opin Neurol 23:394–400 [PubMed: 20610990]
17. Dickson DW, Kouri N, Murray ME, Josephs KA (2011) Neuropathology of frontotemporal lobar degeneration-tau (FTLD-tau). J Mol Neurosci 45:384–389 [PubMed: 21720721]
18. Eisele YS, Obermüller U, Heilbronner G, Baumann F, Kaeser SA, Wolburg H et al. (2010) Peripherally applied Abeta-containing inoculates induce cerebral beta-amyloidosis. Science 330:980–982 [PubMed: 20966215]
19. Falcon B, Zhang W, Murzin AG, Murshudov G, Garringer HJ, Vidal R et al. (2018) Structures of filaments from Pick's disease reveal a novel tau protein fold. Nature 561:137–140 [PubMed: 30158706]
20. Fan L, Li H, Zhuo J, Zhang Y, Wang J, Chen L et al. (2016) The human brainnetome atlas: a new brain atlas based on connectional architecture. Cereb Cortex 26:3508–3526 [PubMed: 27230218]
21. Gardner RC, Boxer AL, Trujillo A, Mirsky JB, Guo CC, Gennatas ED et al. (2013) Intrinsic connectivity network disruption in progressive supranuclear palsy. Ann Neurol 73:603–616 [PubMed: 23536287]
22. Goedert M (2015) Neurodegeneration. Alzheimer's and Parkinson's diseases: the prion concept in relation to assembled Aβ, tau, and α-synuclein. Science 349:1255555 [PubMed: 26250687]
23. Gorno-Tempini ML, Hillis AE, Weintraub S, Kertesz A, Mendez M, Cappa SF et al. (2011) Classification of primary progressive aphasia and its variants. Neurology 76:1006–1014 [PubMed: 21325651]
24. Guo JL, Lee VM (2013) Neurofibrillary tangle-like tau pathology induced by synthetic tau fibrils in primary neurons over-expressing mutant tau. FEBS Lett 587:717–723 [PubMed: 23395797]
25. Habas C, Cabanis EA (2007) Anatomical parcellation of the brainstem and cerebellar white matter: a preliminary probabilistic tractography study at 3 T. Neuroradiology 49:849–863 [PubMed: 17701168]
26. Hof PR, Bouras C, Perl DP, Morrison JH (1994) Quantitative neuropathologic analysis of Pick's disease cases: cortical distribution of Pick bodies and coexistence with Alzheimer's disease. Acta Neuropathol 87:115–124 [PubMed: 8171960]
27. Hyman BT, Phelps CH, Beach TG, Bigio EH, Cairns NJ, Carrillo MC et al. (2012) National Institute on Aging-Alzheimer's Association guidelines for the neuropathologic assessment of Alzheimer's disease. Alzheimers Dement 8:1–13 [PubMed: 22265587]
28. Iba M, Guo JL, McBride JD, Zhang B, Trojanowski JQ, Lee VM (2013) Synthetic tau fibrils mediate transmission of neurofibrillary tangles in a transgenic mouse model of Alzheimer's-like tauopathy. J Neurosci 33:1024–1037 [PubMed: 23325240]
29. Jackson SJ, Kerridge C, Cooper J, Cavallini A, Falcon B, Cella CV et al. (2016) Short fibrils constitute the major species of seed-competent tau in the brains of mice transgenic for human P301S tau. J Neurosci 36:762–772 [PubMed: 26791207]
30. Kaufman SK, Sanders DW, Thomas TL, Ruchinskas AJ, Vaquer-Alicea J, Sharma AM et al. (2016) Tau prion strains dictate patterns of cell pathology, progression rate, and regional vulnerability in vivo. Neuron 92:796–812 [PubMed: 27974162]
31. Kim E-J, Vatsavayai S, Seeley WW (2017) Neuropathology of dementia. Cambridge university press, Cambridge

Author Manuscript Author Manuscript Author Manuscript Author Manuscript

32. Kim EJ, Brown JA, Deng J, Hwang JL, Spina S, Miller ZA et al. (2018) Mixed TDP-43 proteinopathy and tauopathy in frontotemporal lobar degeneration: nine case series. J Neurol 265:2960–2971 [PubMed: 30324308]
33. Lee SE, Rabinovici GD, Mayo MC, Wilson SM, Seeley WW, DeArmond SJ et al. (2011) Clinicopathological correlations in corticobasal degeneration. Ann Neurol 70:327–340 [PubMed: 21823158]
34. Ling H, Kovacs GG, Vonsattel JP, Davey K, Mok KY, Hardy J et al. (2016) Astrogliopathy predominates the earliest stage of corticobasal degeneration pathology. Brain 139:3237–3252 [PubMed: 27797812]
35. Litvan I, Agid Y, Calne D, Campbell G, Dubois B, Duvoisin RC et al. (1996) Clinical research criteria for the diagnosis of progressive supranuclear palsy (Steele-Richardson-Olszewski syndrome): report of the NINDS-SPSP international workshop. Neurology 47:1–9 [PubMed: 8710059]
36. Liu L, Drouet V, Wu JW, Witter MP, Small SA, Clelland C et al. (2012) Trans-synaptic spread of tau pathology in vivo. PLoS ONE 7:e31302 [PubMed: 22312444]
37. Mackenzie I, Neumann M, Bigio E, Cairns N, Alafuzoff I, Kril J et al. (2010) Nomenclature and nosology for neuropathologic subtypes of frontotemporal lobar degeneration: an update. Acta Neuropathol 119:1–4 [PubMed: 19924424]
38. McKeith IG, Dickson DW, Lowe J, Emre M, O'Brien JT, Feldman H et al. (2005) Diagnosis and management of dementia with Lewy bodies: third report of the DLB Consortium. Neurology 65:1863–1872 [PubMed: 16237129]
39. McKhann G, Drachman D, Folstein M, Katzman R, Price D, Stadlan E (1984) Clinical diagnosis of Alzheimer's disease: report of the NINCDS-ADRDA Work Group under the auspices of Department of Health and Human Services Task Force on Alzheimer's Disease. Neurology 34:939–944 [PubMed: 6610841]
40. McKhann GM, Knopman DS, Chertkow H, Hyman BT, Jack CR, Kawas CH et al. (2011) The diagnosis of dementia due to Alzheimer's disease: recommendations from the National Institute on Aging-Alzheimer's Association workgroups on diagnostic guidelines for Alzheimer's disease. Alzheimers Dement 7:263–269 [PubMed: 21514250]
41. Meyer-Luehmann M, Coomaraswamy J, Bolmont T, Kaeser S, Schaefer C, Kilger E et al. (2006) Exogenous induction of cerebral beta-amyloidogenesis is governed by agent and host. Science 313:1781–1784 [PubMed: 16990547]
42. Miki Y, Mori F, Tanji K, Kurotaki H, Kakita A, Takahashi H et al. (2014) An autopsy case of incipient Pick's disease: immunohistochemical profile of early-stage Pick body formation. Neuropathology 34:386–391 [PubMed: 24444359]
43. Montine TJ, Phelps CH, Beach TG, Bigio EH, Cairns NJ, Dickson DW et al. (2012) National Institute on Aging-Alzheimer's Association guidelines for the neuropathologic assessment of Alzheimer's disease: a practical approach. Acta Neuropathol 123:1–11 [PubMed: 22101365]
44. Naidich TP, Duvernoy HM, Delman BN, Sorensen AG, Kollias SS, Haacke EM (2009) Duvernoy's Atlas of the human brain stem and cerebellum. Springer, Vienna, NewYork
45. Narasimhan S, Lee VMY (2017) The use of mouse models to study cell-to-cell transmission of pathological tau. Methods Cell Biol 141:287–305 [PubMed: 28882308]
46. Neary D, Snowden J, Gustafson L, Passant U, Stuss D, Black S et al. (1998) Frontotemporal lobar degeneration: a consensus on clinical diagnostic criteria. Neurology 51:1546–1554 [PubMed: 9855500]
47. Porta S, Xu Y, Restrepo CR, Kwong LK, Zhang B, Brown HJ et al. (2018) Patient-derived frontotemporal lobar degeneration brain extracts induce formation and spreading of TDP-43 pathology in vivo. Nat Commun 9:4220 [PubMed: 30310141]
48. Prusiner SB (1982) Novel proteinaceous infectious particles cause scrapie. Science 216:136–144 [PubMed: 6801762]
49. Rahimi J, Milenkovic I, Kovacs GG (2015) Patterns of tau and α-synuclein pathology in the visual system. J Parkinsons Dis 5:333–340 [PubMed: 25737267]
50. Raj A, Kuceyeski A, Weiner M (2012) A network diffusion model of disease progression in dementia. Neuron 73:1204–1215 [PubMed: 22445347]

Author Manuscript Author Manuscript Author Manuscript Author Manuscript

51. Raman MR, Kantarci K, Murray ME, Jack CR, Vemuri P (2016) Imaging markers of cerebrovascular pathologies: pathophysiology, clinical presentation, and risk factors. Alzheimers Dement (Amst) 5:5–14 [PubMed: 28054023]
52. Rascovsky K, Hodges JR, Knopman D, Mendez MF, Kramer JH, Neuhaus J et al. (2011) Sensitivity of revised diagnostic criteria for the behavioural variant of frontotemporal dementia. Brain 134:2456–2477 [PubMed: 21810890]
53. Rebeiz JJ, Kolodny EH, Richardson EP Jr (1968) Corticodentatonigral degeneration with neuronal achromasia. Arch Neurol 18:20–33 [PubMed: 5634369]
54. Rorden C, Brett M (2000) Stereotaxic display of brain lesions. Behav Neurol 12:191–200 [PubMed: 11568431]
55. Sanders DW, Kaufman SK, DeVos SL, Sharma AM, Mirbaha H, Li A et al. (2014) Distinct tau prion strains propagate in cells and mice and define different tauopathies. Neuron 82:1271–1288 [PubMed: 24857020]
56. Santos-Santos MA, Mandelli ML, Binney RJ, Ogar J, Wilson SM, Henry ML et al. (2016) Features of patients with nonfluent/agrammatic primary progressive aphasia with underlying progressive supranuclear palsy pathology or corticobasal degeneration. JAMA Neurol 73:733–742 [PubMed: 27111692]
57. Schmahmann JD, Ko R, MacMore J (2004) The human basis pontis: motor syndromes and topographic organization. Brain 127:1269–1291 [PubMed: 15128614]
58. Schmahmann JD, Pandya DN (1997) Anatomic organization of the basilar pontine projections from prefrontal cortices in rhesus monkey. J Neurosci 17:438–458 [PubMed: 8987769]
59. Schmahmann JD, Pandya DN (1989) Anatomical investigation of projections to the basis pontis from posterior parietal association cortices in rhesus monkey. J Comp Neurol 289:53–73 [PubMed: 2478597]
60. Schmahmann JD, Pandya DN (1995) Prefrontal cortex projections to the basilar pons in rhesus monkey: implications for the cerebellar contribution to higher function. Neurosci Lett 199:175–178 [PubMed: 8577391]
61. Schmahmann JD, Pandya DN (1993) Prelunate, occipitotemporal, and parahippocampal projections to the basis pontis in rhesus monkey. J Comp Neurol 337:94–112 [PubMed: 8276995]
62. Schmahmann JD, Rosene DL, Pandya DN (2004) Motor projections to the basis pontis in rhesus monkey. J Comp Neurol 478:248–268 [PubMed: 15368534]
63. Seeley W, Crawford R, Zhou J, Miller B, Greicius M (2009) Neurodegenerative diseases target large-scale human brain networks. Neuron 62:42–52 [PubMed: 19376066]
64. Seeley WW (2017) Mapping neurodegenerative disease onset and progression. Cold Spring Harb Perspect Biol 9
65. Stieltjes B, Kaufmann WE, van Zijl PC, Fredericksen K, Pearlson GD, Solaiyappan M et al. (2001) Diffusion tensor imaging and axonal tracking in the human brainstem. Neuroimage 14:723–735 [PubMed: 11506544]
66. Tartaglia M, Sidhu M, Laluz V, Racine C, Rabinovici G, Creighton K et al. (2010) Sporadic corticobasal syndrome due to FTLD-TDP. Acta Neuropathol 119:365–374 [PubMed: 19876635]
67. Tredici G, Barajon I, Pizzini G, Sanguineti I (1990) The organization of corticopontine fibres in man. Acta Anat (Basel) 137:320–323 [PubMed: 2368586]
68. Tsuboi Y, Josephs KA, Boeve BF, Litvan I, Caselli RJ, Caviness JN et al. (2005) Increased tau burden in the cortices of progressive supranuclear palsy presenting with corticobasal syndrome. Mov Disord 20:982–988 [PubMed: 15834857]
69. Whitwell JL, Boeve BF, Weigand SD, Senjem ML, Gunter JL, Baker MC et al. (2015) Brain atrophy over time in genetic and sporadic frontotemporal dementia: a study of 198 serial magnetic resonance images. Eur J Neurol 22:745–752 [PubMed: 25683866]
70. Witelson SF (1989) Hand and sex differences in the isthmus and genu of the human corpus callosum. A postmortem morphological study. Brain 112(Pt 3):799–835 [PubMed: 2731030]
71. Wu JW, Herman M, Liu L, Simoes S, Acker CM, Figueroa H et al. (2013) Small misfolded Tau species are internalized via bulk endocytosis and anterogradely and retrogradely transported in neurons. J Biol Chem 288:1856–1870 [PubMed: 23188818]

Author Manuscript Author Manuscript Author Manuscript Author Manuscript

72. Zhou J, Gennatas ED, Kramer JH, Miller BL, Seeley WW (2012) Predicting regional neurodegeneration from the healthy brain functional connectome. Neuron 73:1216–1227 [PubMed: 22445348]

Author Manuscript Author Manuscript Author Manuscript Author Manuscript

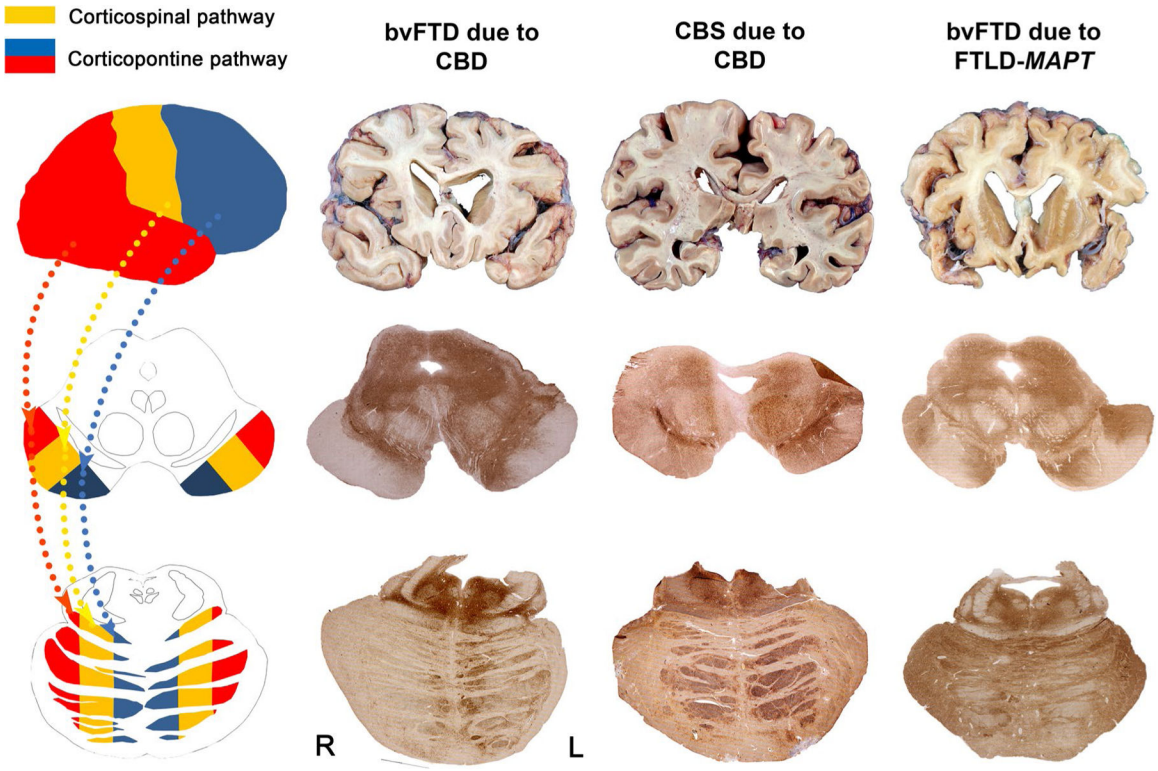

Fig. 1.

Cerebral cortical efferent pathways show predictable axonal tau deposition in bvFTD and CBS: illustrative cases. The schematic diagram (left) demonstrates the cerebral cortical efferent pathways (yellow: corticospinal pathway, blue: prefrontopontine pathway, and red: parieto-temporooccipital pathway) and organization of midbrain cerebral peduncle and basal pontine fibers. Illustrative cases highlighting the relationship between cortical atrophy and brainstem tau deposition patterns in bvFTD and CBS are shown to the right

Author Manuscript Author Manuscript Author Manuscript Author Manuscript

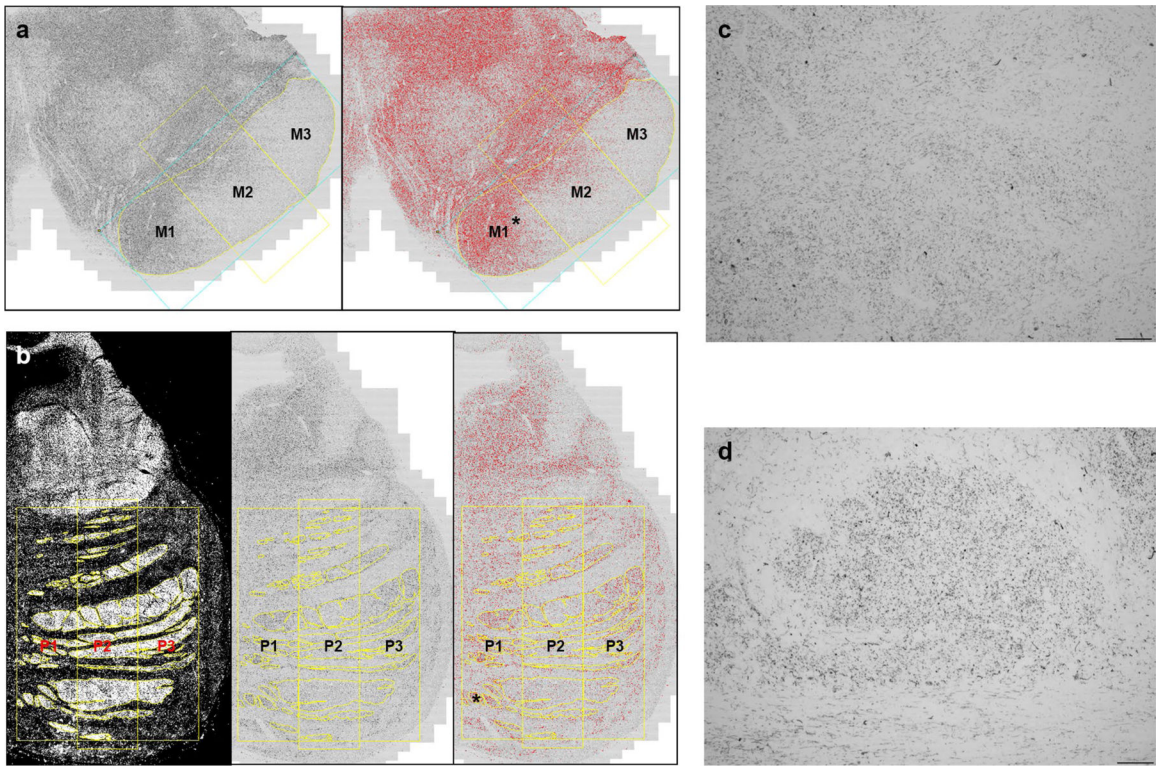

Fig. 2.

Region-of-interest delineation for the midbrain cerebral peduncle and pontine fibers. Midbrain cerebral peduncle (**a**) was divided into three portions (yellow line) based on a one-dimensional geometric baseline connecting the most medial (M1) and lateral points (M3) of the peduncle (blue rectangle). Basal pontine descending fibers were divided into three portions, P1, P2, and P3, from medial to lateral. The ROIs were drawn on the eight bit black and white image for midbrain (**a**, left) and the darkfield images for pons (**b**, left), which were transposed into black and white images (**b**, middle). After adjusting the Yen algorithm to a threshold (**a**, right; **b**, right), the tau area fraction (%) for each of ROI was obtained. High magnification views of asterisk in **a**, **b** show that the tau staining within the midbrain (**c**) and pontine (**d**) ROIs appears as predominantly small dotlike structures, suggesting axially cut descending axons. In general, the degree of staining within potentially non-axonal structures was correlated with the degree of axonal tau staining

Author Manuscript Author Manuscript Author Manuscript Author Manuscript

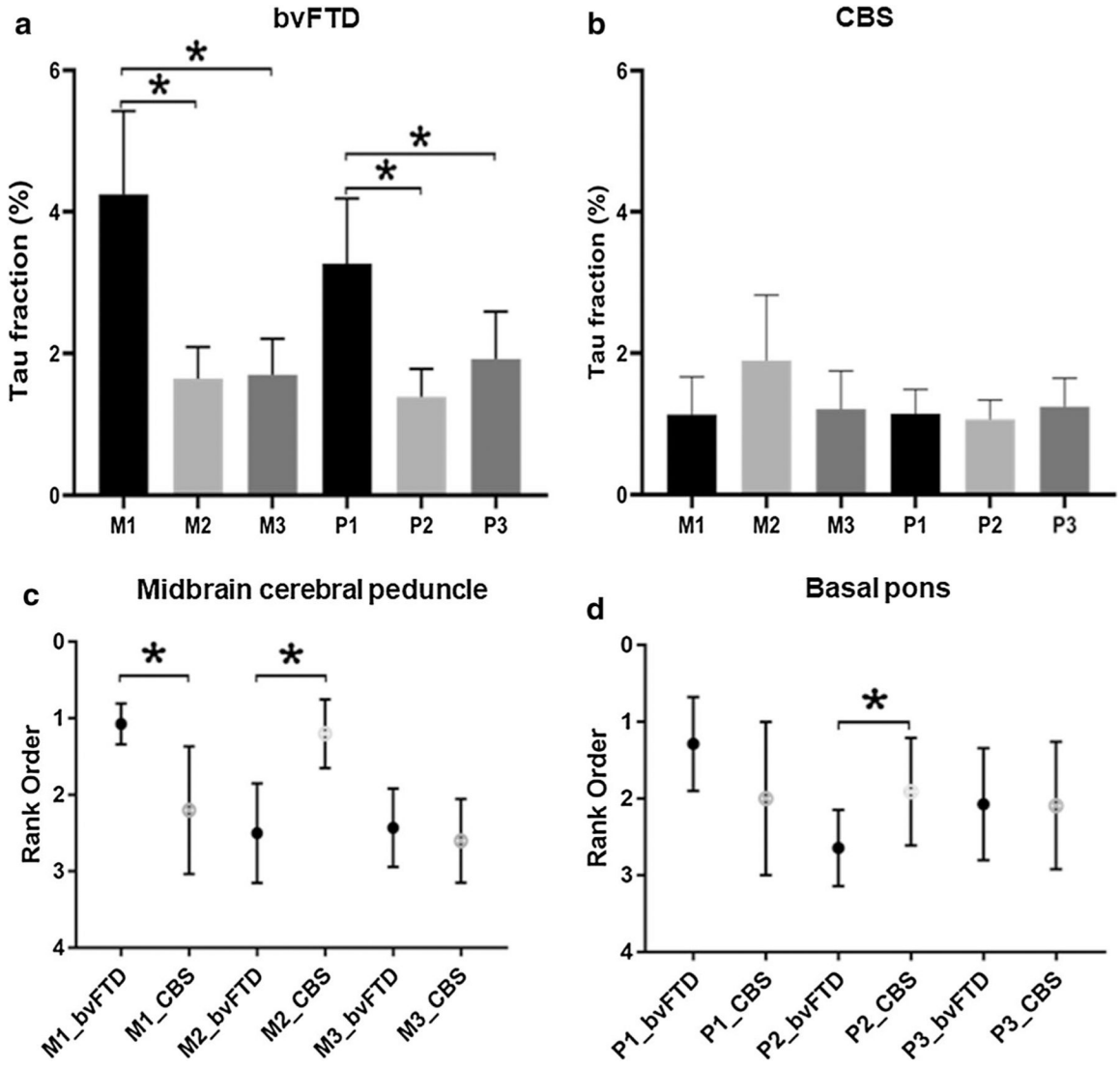

Fig. 3.

Quantitative subregional tau deposition in midbrain cerebral peduncle and basal pons in bvFTD (**a**) vs. CBS (**b**) (*$p < 0.05$ M1 vs M2, M1 vs M3, P1 vs P2, P1 vs P3). The rank order of subregional tau deposition in midbrain cerebral peduncle (**c**) and basal pons (**d**) in bvFTD and CBS (*$p < 0.05$)

Author Manuscript Author Manuscript Author Manuscript Author Manuscript

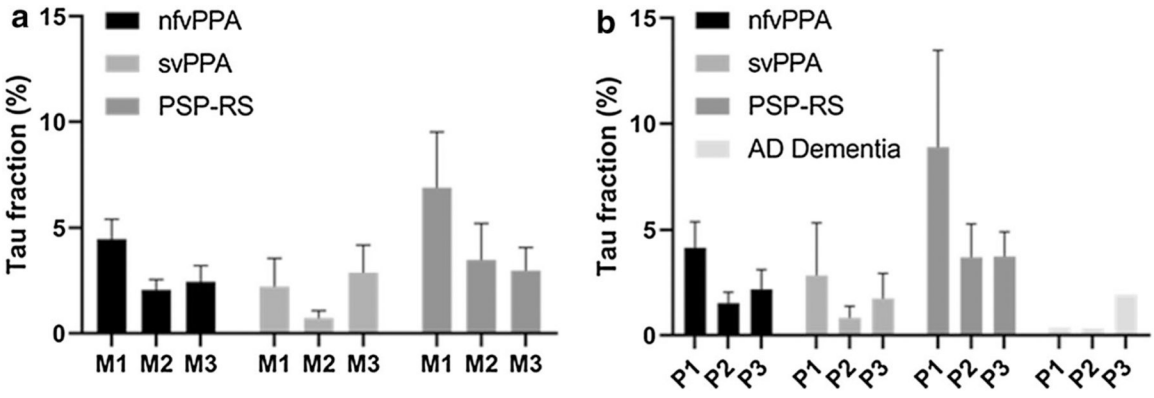

Fig. 4.

Each of these four clinical syndromic groups, though too small to analyze statistically, shows a predictable pattern of quantitative tau deposition in midbrain cerebral peduncle (**a**) and basal pons (**b**)

Author Manuscript Author Manuscript Author Manuscript Author Manuscript

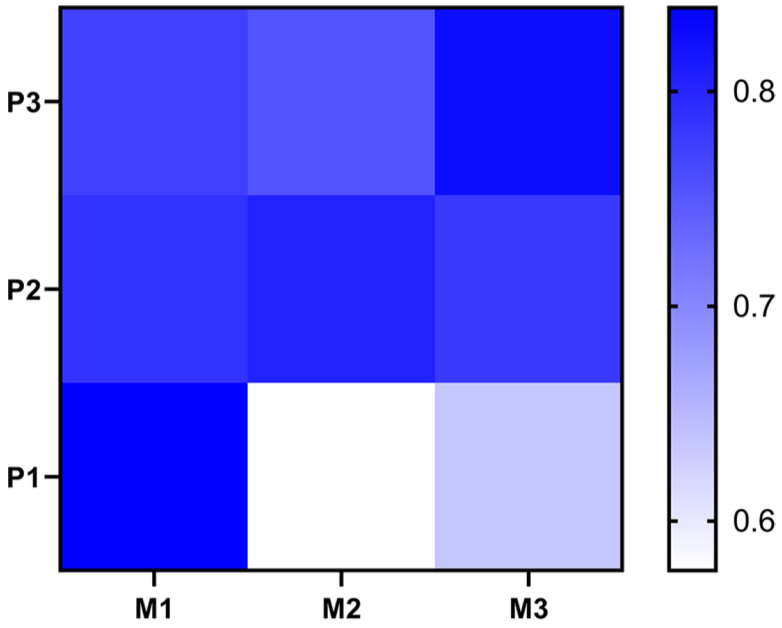

Fig. 5.

A heat map showing the correlations between the six ROIs of midbrain cerebral peduncle and basal pons. The strongest correlations between M1vs. P1, M2 vs. P2, and M3 vs. P3 suggest that tau from the same cortical sources spreads along the efferent axonal pathway. Even the lowest correlations are nonetheless high, as might be expected, since regions in all three sectors are typically affected to some degree in each patient

Author Manuscript Author Manuscript Author Manuscript Author Manuscript

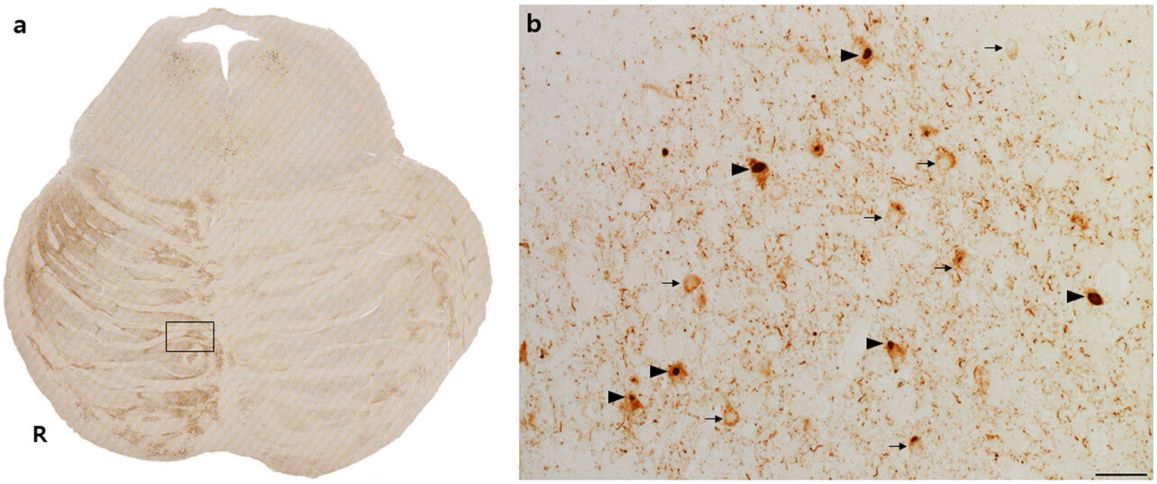

Fig. 6.

Tau neuronal cytoplasmic inclusions within pontine nuclei correlate with regions of higher axonal tau burden. This representative patient with bvFTD due to Pick's disease shows an asymmetric rightward P1 and P3 tau involvement pattern (**a**). Box in **a** is magnified in **b** (scale bar 25 μm) to show frequent diffuse NCIs (arrows) and Pick bodies (arrowheads) in pontine nucleus neurons, alongside tau-positive descending axons, which appear as dots in the axial plane (**b**)

Author Manuscript Author Manuscript Author Manuscript Author Manuscript

Acta Neuropathol. Author manuscript; available in PMC 2020 February 11.

Table 1

Patient demographic and pathological features

Case #	Pathological Dx	Clinical Dx	Sex	Age at onset	Age at death	Disease duration (years)	PMI (hours)	ADNC	LBD	TDP-43[a]	VBI	Lacunes	Microinfarcts	Mid-brain section	Pons section
1	PiD	bvFTD	F	54	60	6	15.1	A1B1C2	−	−	−	−	−	+	+
2	PiD	bvFTD	M	51	57	6	21.7	A0B0C0	−	−	−	−	−	+	+
3	PiD	bvFTD	M	60	70	10	10.2	A1B0C2	−	−	−	−	−	+	−
4	PiD	bvFTD	M	63	72	9	24.3	A0B0C0	−	−	−	−	−	+	+
5	PiD	bvFTD	F	63	76	13	25.5	A0B0C0	−	−	+	−	GP, Putamen AG	+	+
6	PiD	bvFTD	F	56	69	13	6.3	A0B0C0	−	−	−	−	−	+	+
7	PiD	bvFTD	M	53	57	4	12.4	A1B1C0	−	−	−	−	−	+	+
8	PiD	CBS	M	59	64	5	13.7	A1B0C0	Brainstem	−	−	−	−	+	+
9	PiD	CBS	F	58	71	13	69.0	A1B1C1	Brainstem	−	+	−	MIC	+	+
10	PiD	nfvPPA	M	65	73	8	7.9	A1B1C3	−	−	+	−	ITG, AMG, Putamen, ERC	−	+
11	PiD	nfvPPA	F	54	63	9	4.3	A0B0C0	−	−	−	−	−	+	+
12	PiD	nfvPPA	F	66	74	8	9.8	A0B0C0	−	Limbic	+	−	FP, MIC	−	+
13	PiD	nfvPPA	M	49	60	11	15.2	A0B0C0	−	−	−	−	−	+	+
14	PiD	svPPA	M	60	71	11	<8	A1B0C0	−	−	−	−	−	+	+
15	PiD	svPPA	M	52	63	11	14.5	A1B0C0	−	−	−	−	−	−	+
16	PiD	AD Dementia	F	58	67	9	6.8	A1B1C2	Brainstem	−	+	BG	AOG, ACC, MFG, IFG, SCC, ITG, AMG, GP, Putamen, SFS	−	+
17	CBD	bvFTD	M	77	83	6	4.0	A2B2C3	−	−	+	−	GP	−	+
18	CBD	bvFTD	M	57	63	6	6.2	A1B1C3	−	−	−	−	−	+	+
19	CBD	bvFTD	M	59	71	12	7.6	A0B0C0	−	Limbic	−	−	−	+	+
20	CBD	bvFTD	M	57	65	8	4.5	A1B1C0	−	−	−	−	−	+	+
21	CBD	bvFTD	F	64	72	8	11.8	A3B1C3	−	−	+	−	GP, Putamen	+	+
22	CBD	CBS	M	61	68	7	7.4	A1B0C0	−	−	+	−	MIC, Claustrum, Putamen	+	+
23	CBD	CBS	F	57	62	5	6.5	A1B1C0	−	−	+	−	Putamen	−	+

Author Manuscript Author Manuscript Author Manuscript Author Manuscript

Case #	Pathological Dx	Clinical Dx	Sex	Age at onset	Age at death	Disease duration (years)	PMI (hours)	ADNC	LBD	TDP-43[a]	VBI	Lacunes	Microinfarcts	Mid-brain section	Pons section
24	CBD	CBS	M	61	66	5	12.1	A1B1C0	Brainstem	−	−	−	−	−	+
25	CBD	CBS	F	59	64	5	8.6	A1B1C0	−	−	−	−	−	+	+
26	CBD	CBS	M	68	73	5	8.2	A1B1C0	Brainstem	−	−	−	−	+	+
27	CBD	CBS	F	57	63	6	5.0	A0B1C0	Brainstem	−	−	−	−	−	+
28	CBD	CBS	F	69	77	8	11.7	A1B1C2	−	−	+	−	ACC, IFG, Claustrum, HC, STG/MTG, AG	−	+
29	CBD	CBS	F	57	64	7	7.8	A0B1C0	−	−	+	−	Putamen	−	+
30	CBD	CBS	F	55	63	8	5.8	A1B1C0	−	−	−	−	−	−	+
31	CBD	PSP-RS	M	56	60	4	10.3	A1B1C1	−	−	−	−	−	+	+
32	CBD	PSP-RS	F	63	67	4	7.7	A1B1C2	−	−	−	−	−	+	+
33	CBD	PSP-RS	F	60	64	4	6.1	A0B1C0	−	−	−	−	−	+	+
34	CBD	nfvPPA	F	63	69	6	<8	A1B1C1	Brainstem	−	+	Putamen	ACC, MFG, VS, ITG, AMG, MIC, Claustrum, Putamen, Thalamus	−	+
35	CBD	nfvPPA	F	61	70	9	7.4	A1B2C0	−	−	−	−	−	+	+
36	CBD	nfvPPA	F	48	69	21	14.6	A1B1C0	−	−	+	−	ACC, Claustrum, Putamen, Thalamus	+	+
37	CBD	svPPA	M	66	72	6	36.0	A1B1C3	−	−	−	−	−	+	+
38	FTLD-tau/ *MAPT* (P301L)	bvFTD	F	46	63	17	19.7	A1B0C0	−	−	−	−	−	+	+
39	FTLD-tau/ *MAPT* (P301L)	bvFTD	F	55	59	4	24.2	A1B1C0	−	−	−	−	−	+	+
40	FTLD-tau/ *MAPT* (P301L)	bvFTD	M	66	75	9	8.6	A1B1C0	−	Limbic	−	−	−	+	+

AD Alzheimer's disease, *ACC* anterior cingulate cortex, *ADNC* Alzheimer's disease neuropathological changes, *AG* angular gyrus, *AMG* amygdala, *AOG* anterior orbital gyrus, *BG* basal ganglia, *bvFTD* behavioral variant of frontotemporal dementia, *CBD* corticobasal degeneration, *CBS* corticobasal syndrome, *Dx.* diagnosis, *ERC* entorhinal cortex, *F* female, *FP* frontal pole, *FTLD* frontotemporal lobar degeneration, *GP* globus pallidus, *HC* hippocampus, *IFG* inferior frontal gyrus, *ITG* inferior temporal gyrus, *LBD* Lewy body disease, *M* male, *MAPT* microtubule- associated protein tau, *MFG* middle frontal gyrus, *MIC* middle insular cortex, *nfvPPA* nonfluent variant of primary progressive aphasia, *PMI* postmortem interval, *PiD* Pick's disease *PSP-RS* progressive supranuclear palsy-Richardson syndrome, *SCC* subgenual cingulate cortex, *SFS* superior frontal sulcus, *STG/MTG* superior temporal gyrus/middle temporal gyrus, *svPPA* semantic variant of primary progressive aphasia, *TDP-43* TAR DNA-binding protein of 43 kDa, *VBI* vascular brain injuries, *VS* ventral striatum, + available, − not available

Author Manuscript

[a]TDP-43 refers to limbic-predominant age-related TDP-43 disease

Author Manuscript

Author Manuscript

Author Manuscript

Author Manuscript Author Manuscript Author Manuscript Author Manuscript

Table 2

Cortical degeneration and tau inclusion burden

Subregion	Tau score			Neurodegeneration score			Composite tau + neurodegeneration score			Regional atrophy score		
	Frontal	Perirolandic	PTO	Frontal	Perirolandic	PTO	Frontal	Perirolandic	PTO	Frontal	Perirolandic	PTO
Midbrain subjects												
bvFTD-PiD (*n* = 7)	2.1 ± 0.2	0.8 ± 0.4	1.8 ± 0.4	3.5 ± 0.8	0.5 ± 0.6	2.5 ± 1.0	5.0 ± 0.9	1.3 ± 0.8	4.0 ± 1.1	3.5 ± 1.6 (*n* = 7)	0.6 ± 1.4 (*n* = 7)	2.6 ± 1.3 (*n* = 7)
bvFTD-CBD (*n* = 4)	2.0 ± 0.2	1.6 ± 0.2	1.6 ± 0.1	1.6 ± 0.1	1.0 ± 0.9	0.8 ± 0.5	2.8 ± 0.5	2.6 ± 1.1	2.1 ± 0.8	2.4 ± 0.9 (*n* = 4)	1.1 ± 0.9 (*n* = 4)	1.0 ± 0.9 (*n* = 4)
bvFTD- FTLD-tau/*MAPT* (*n* = 3)	1.4 ± 0.1	0.8 ± 0.6	1.2 ± 0.1	3.7 ± 1.0	0.8 ± 0.6	2.8 ± 0.4	4.7 ± 1.0	1.6 ± 0.7	4.0 ± 0.4	4.2 (*n* = 1)	2.6 (*n* = 1)	2.8 (*n* = 1)
bvFTD-overall (*n* = 14)	1.9 ± 0.3	1.0 ± 0.5	1.7 ± 0.4	3.0 ± 1.2	0.7 ± 0.7	2.1 ± 1.1	4.3 ± 1.2	1.7 ± 1.0	3.5 ± 1.2	3.2 ± 1.4 (*n* = 12)	0.9 ± 1.3 (*n* = 12)	2.1 ± 1.3 (*n* = 12)
CBS-PiD (*n* = 2)	2.2 ± 0.0	1.8 ± 0.6	1.3 ± 0.3	3.5 ± 0.6	2.9 ± 1.6	2.5 ± 0.3	4.7 ± 0.6	4.7 ± 2.2	3.8 ± 0.6	3.1 ± 1.9 (*n* = 2)	2.7 ± 0.5 (*n* = 2)	2.5 ± 1.4 (*n* = 2)
CBS-CBD (*n* = 3)	1.5 ± 0.2	1.6 ± 0.3	0.9 ± 0.1	0.8 ± 0.6	2.1 ± 0.6	0.4 ± 0.5	1.6 ± 0.6	3.7 ± 0.3	1.2 ± 0.5	1.4 ± 0.4 (*n* = 2)	1.8 ± 0.3 (*n* = 2)	1.2 ± 0.2 (*n* = 2)
CBS-overall (*n* = 5)	1.8 ± 0.4	1.7 ± 0.4	1.1 ± 0.3	1.9 ± 1.6	2.4 ± 1.0	1.2 ± 1.2	2.8 ± 1.8	4.1 ± 1.2	2.2 ± 1.5	2.2 ± 1.5 (*n* = 4)	2.2 ± 0.6 (*n* = 4)	1.8 ± 1.1 (*n* = 4)
Pons subjects												
bvFTD-PiD (*n* = 6)	2.1 ± 0.3	0.8 ± 0.4	1.8 ± 0.4	3.5 ± 0.9	0.6 ± 0.7	2.6 ± 1.1	4.9 ± 0.9	1.4 ± 0.9	4.0 ± 1.2	3.4 ± 1.7 (*n* = 6)	0.6 ± 1.5 (*n* = 6)	2.7 ± 1.4 (*n* = 6)
bvFTD-CBD (*n* = 5)	2.0 ± 0.2	1.5 ± 0.3	1.6 ± 0.1	1.6 ± 0.2	0.9 ± 0.8	0.9 ± 0.5	2.7 ± 0.5	2.4 ± 1.0	2.2 ± 0.7	2.4 ± 0.9 (*n* = 4)	1.1 ± 0.9 (*n* = 4)	1.0 ± 0.9 (*n* = 4)
bvFTD- FTLD-tau/*MAPT* (*n* = 3)	1.4 ± 0.1	0.8 ± 0.6	1.2 ± 0.1	3.7 ± 1.0	0.8 ± 0.6	2.8 ± 0.4	4.7 ± 1.0	1.6 ± 0.7	4.0 ± 0.4	4.2 (*n* = 1)	2.6 (*n* = 1)	2.8 (*n* = 1)
bvFTD-overall (*n* = 14)	1.9 ± 0.3	1.1 ± 0.5	1.6 ± 0.4	2.9 ± 1.2	0.8 ± 0.7	2.0 ± 1.2	4.1 ± 1.3	1.8 ± 0.9	3.4 ± 1.2	3.1 ± 1.4 (*n* = 11)	1.0 ± 1.3 (*n* = 11)	2.1 ± 1.4 (*n* = 11)
CBS-PiD (*n* = 2)	2.2 ± 0.0	1.8 ± 0.6	1.3 ± 0.3	3.5 ± 0.6	2.9 ± 1.6	2.5 ± 0.3	4.7 ± 0.6	4.7 ± 2.2	3.8 ± 0.6	3.1 ± 1.9 (*n* = 2)	2.7 ± 0.5 (*n* = 2)	2.5 ± 1.4 (*n* = 2)
CBS-CBD (*n* = 9)	1.4 ± 0.4	1.6 ± 0.4	0.9 ± 0.3	0.9 ± 0.6	1.8 ± 0.5	0.5 ± 0.5	1.6 ± 0.7	3.4 ± 0.7	1.2 ± 0.6	1.4 ± 0.6 (*n* = 7)	2.0 ± 0.8 (*n* = 7)	1.0 ± 0.7 (*n* = 7)
CBS-overall (*n* = 11)	1.6 ± 0.5	1.6 ± 0.4	0.9 ± 0.3	1.3 ± 1.2	2.0 ± 0.8	0.8 ± 0.9	2.2 ± 1.4	3.6 ± 1.1	1.6 ± 1.2	1.8 ± 1.2 (*n* = 9)	2.2 ± 0.8 (*n* = 9)	1.3 ± 1.0 (*n* = 9)

bvFTD behavioral variant of frontotemporal dementia, *CBD* corticobasal degeneration, *CBS* corticobasal syndrome, *FTLD* frontotemporal lobar degeneration, *MAPT* microtubule-associated protein tau, *PiD* Pick's disease, *PTO* parieto-temporooccipital

Author Manuscript Author Manuscript Author Manuscript Author Manuscript

Table 3

Cortical atrophy assessed with antemortem MRI correlates with cortical degeneration of post-mortem histology

Subregion	Tau score			Neurodegeneration score			Composite tau + neurodegeneration score		
	Frontal	**Perirolandic**	**PTO**	**Frontal**	**Perirolandic**	**PTO**	**Frontal**	**Perirolandic**	**PTO**
Regional atrophy score									
Frontal									
ρ	**0.532**	− 0.598	**0.525**	**0.444**	− 0.381	0.279	**0.385**	− 0.437	**0.350**
P	**0.001**§	< 0.001	**0.002**§	**0.010**§	0.029	0.116	**0.027**§	0.011	**0.046**
Perirolandic									
ρ	− 0.418	**0.887**	− 0.824	− 0.557	**0.866**	− 0.704	− 0.510	**0.845**	− 0.802
P	0.016	**< 0.001**§	< 0.001	0.001	**< 0.001**§	< 0.001	0.002	**< 0.001**§	< 0.001
PTO									
ρ	0.114	− 0.687	**0.676**	**0.398**	− 0.800	**0.668**	**0.386**	− 0.749	**0.748**
P	0.423	< 0.001	**< 0.001**§	**0.022**§	< 0.001	**< 0.001**§	**0.027**§	< 0.001	**< 0.001**§

Significant correlations are in bold

PTO parieto-temporooccipital

§ The ones that remain significant after false discovery rate correction for multiple comparisons

Author Manuscript Author Manuscript Author Manuscript Author Manuscript

Table 4

Cortical degeneration and tau inclusion burden correlates with subregional brainstem tau pathology

	Frontal					**Perirolandic**					**PTO**			
	TS	**NS**	**cs**	**AS**		**TS**	**NS**	**CS**	**AS**		**TS**	**NS**	**CS**	**AS**
M1					M2					M3				
ρ	**0.435**	**0.556**	0.339	0.354	ρ	**0.397**	**0.493**	**0.529**	0.352	ρ	− 0.198	0.184	0.135	0.098
P	**0.021**	**0.002** *,§	0.078	0.090	P	**0.037** *	**0.008** *,§	**0.004** *,§	0.092	P	0.313	0.348	0.495	0.650
P1					P2					P3				
ρ	**0.558**	**0.507**	0.313	**0.506**	ρ	0.297	0.284	**0.340**	0.296	ρ	− 0.053	0.197	0.203	0.165
P	0.000 *,§	**0.001** *,§	0.052	**0.003** *,§	P	0.070	0.080	**0.034**	0.100	P	0.748	0.230	0.216	0.368

Significant correlations are in bold

AS atrophic score, *CS* composite score, *NS* neurodegeneration score, *PTO* parieto-temporo-occipital, *TS* tau score

*The *p* values that remain significant after removing all glial scores

§The *p* values that remain significant after false discovery rate correction for multiple comparisons